



HAL
open science

Co-production of hydrogen and carbon black from solar thermal methane splitting in a tubular reactor prototype

Sylvain Rodat, Stéphane Abanades, Gilles Flamant

► To cite this version:

Sylvain Rodat, Stéphane Abanades, Gilles Flamant. Co-production of hydrogen and carbon black from solar thermal methane splitting in a tubular reactor prototype. *Solar Energy*, 2011, 85 (4), pp.645-652. 10.1016/j.solener.2010.02.016 . hal-02567199v2

HAL Id: hal-02567199

<https://hal.science/hal-02567199v2>

Submitted on 4 May 2022

HAL is a multi-disciplinary open access archive for the deposit and dissemination of scientific research documents, whether they are published or not. The documents may come from teaching and research institutions in France or abroad, or from public or private research centers.

L'archive ouverte pluridisciplinaire **HAL**, est destinée au dépôt et à la diffusion de documents scientifiques de niveau recherche, publiés ou non, émanant des établissements d'enseignement et de recherche français ou étrangers, des laboratoires publics ou privés.

CO-PRODUCTION OF HYDROGEN AND CARBON BLACK FROM SOLAR THERMAL METHANE SPLITTING IN A TUBULAR REACTOR PROTOTYPE

Sylvain Rodat, Stéphane Abanades, and Gilles Flamant

PROMES-CNRS Laboratory, 7 rue du four solaire 66120 FONT-ROMEUE, FRANCE, Phone: +33 4 68 30 77 31, Fax: +33 4 68 30 29 40, E-mail: sylvain.rodatt@promes.cnrs.fr

Abstract

This study addresses the solar thermal decomposition of natural gas for the co-production of hydrogen and Carbon Black (CB) as a high-value nano-material with the bonus of zero CO₂ emission. The work focused on the development of a medium-scale solar reactor (10 kW) based on the indirect heating concept. The solar reactor is composed of a cubic cavity receiver (20 cm-side), which absorbs concentrated solar irradiation through a quartz window by a 9 cm-diameter aperture. The reacting gas flows inside four graphite tubular reaction zones that are settled vertically inside the cavity. Experimental results in the temperature range 1740K – 2070K are presented: acetylene (C₂H₂) was the most important by-product with a mole fraction of up to about 7%, depending on the gas residence time. C₂H₂ content in the off-gas affects drastically the carbon yield of the process. The effects of temperature and residence time are analyzed. A preliminary process study concerning a 55 MW solar chemical plant is proposed on the basis of a process flow sheet. Results show that 1.7 t/h of hydrogen and 5 t/h of CB could be produced with an hydrogen cost competitive to conventional steam methane reforming.

Keywords: Solar energy, methane cracking, carbon black, hydrogen, process economics.

1. Introduction

In order to counter the rising CO₂ emissions, the decarbonisation of fossil fuels is required and the ultimate step is the hydrogen production. Hydrogen appears as one of the most promising energy carriers along with electricity. Natural gas (mainly composed of methane) may play a major role on the way towards a carbon free energy (DOE, 1999). It is the cleanest hydrocarbon fuel (highest H/C ratio) and it can benefit from transportation infrastructures. Nowadays, hydrogen is mainly produced via steam methane reforming (SMR) (Dahl et al., 2004a) while Carbon Black (CB) is principally produced from the furnace process (Donnet et al., 1993). Both processes release large amounts of CO₂ in the atmosphere. It is estimated that steam methane reforming produces 11.9 kg CO₂ eq. per kg of hydrogen produced and the furnace process about 5.7 kg CO₂ eq. per kg of CB produced. Solar thermal methane cracking can be a solution for the clean co-production of hydrogen and carbon black. About 92% of the pollution associated with the two conventional processes can thus be eliminated (Wyss et al., 2007). The overall reaction can be written as:



$$\Delta H^\circ = 75 \text{ kJ}\cdot\text{mol}^{-1} \text{ (216 kJ}\cdot\text{mol}^{-1} \text{ for CH}_4 \text{ at 298K and products at 2000K)}$$

Nevertheless, a more complex reaction scheme must be used to explain the production of by-products such as C₂H₂, C₂H₄, C₂H₆, and more complex molecules like polycyclic aromatic hydrocarbons (PAH). The kinetic mechanism can be described either as a simplified stepwise dehydrogenation: 2CH₄ → C₂H₆ → C₂H₄ → C₂H₂ → C (Back and Back, 1983) or as a more complex scheme including a free radical mechanism composed of 36 and 119 reactions as proposed by Olsvik et al. (1995) and Billaud et al. (1992), respectively. A kinetic study of methane decomposition in a tubular solar reactor along with numerical simulations of the reactor were presented previously (Rodat et al., 2009a, 2009b). At thermodynamic equilibrium, the methane dissociation is complete for temperatures above 1500K (Hirsch et al., 2001).

Special interest was given to solar methane thermal cracking for hydrogen production during the last years.

Two possible reactor designs were investigated, the direct (Kogan and Kogan, 2003; Trommer et al., 2004; Kogan et al., 2004; Hirsch and Steinfeld, 2004; Abanades and Flamant, 2008) and the indirect heating concepts (Dahl et al., 2004a; Wyss et al., 2007; Dahl et al., 2004b). In the indirect heating configuration, the solar irradiated zone is separated from the reacting flow thereby avoiding the particle deposition issue on the window, whereas the direct irradiation of reactants provides an efficient means of heat transfer directly to the reaction site but particle seeding is required for efficient gas heating. This work reports on the results obtained with a 10 kW indirectly heated reactor prototype featuring a cubic graphite cavity (behaving as a black body cavity) with 4 vertical inside tubular reaction zones. This design enables the control of the reactor tube temperature and is also suitable for scaling-up. The design and economic assessment of a commercial solar chemical plant are then outlined.

2. Experimental section

2.1. Experimental set-up

The experimental set-up, shown in Fig. 1, has already been described by Rodat et al. (2009c). It is composed of a 20 cm-side graphite cavity receiver (blackbody absorber of cubic shape). A 9 cm-diameter aperture lets concentrated solar radiation entering within the cavity through an hemispherical quartz window. Thus, the inside cavity swept by nitrogen is separated from ambient oxidizing atmosphere. The reaction takes place in the four tubular graphite zones settled in parallel and vertically in the solar absorber. Each reaction zone, fed independently by a mixture of Ar and CH₄, is composed of two concentric graphite tubes (Fig. 2): an inner tube for gas inlet (12 mm O.D., 4 mm I.D., 345 mm length) and an outer tube for gas outlet (24 mm O.D., 18 mm I.D., 380 mm length, closed at the bottom). The gas enters the inner tube and flows out by the annular space between the outer and inner tubes. The graphite tubes are heated up by both direct solar radiation coming from the aperture and by IR radiation from the cavity walls. The heated tube length inserted in the graphite cavity is about 0.161 m, the remaining part (about 0.203 m-length) corresponds to the insulation zone. Three different insulating layers envelop the reactor cavity in order to limit conduction losses. In total it forms an insulation layer of 0.15 m (0.05 m for each insulating material). The surrounding outer shell of the reactor is made of stainless steel (535x535x373 mm). The reactor is designed for a nominal power of 10 kW and it is set-up at the focus of the 1 MW solar furnace of CNRS-PROMES laboratory. The furnace is composed of a field of 63 heliostats for full power (45 m² per heliostat) and of a parabolic concentrator (1830 m²) delivering up to 9000 suns at the focal plane. During experiments at 10 kW scale, only a fraction of the parabola is used by limiting the number of the sun-tracking heliostats and by using a shutter and a small reactor cavity opening (9 cm-diameter aperture). A photograph of the experimental set-up including the solar reactor is displayed in Fig. 3.

The first experimental step was the heating of the reactor under an argon flow in the tubes. Once the desired temperature is reached, the mixture of argon and methane was injected with a controlled composition. Two mass-flow meters were dedicated to each tube to control accurately the Ar and CH₄ flow-rates. The temperature was measured by a solar blind optical pyrometer (wavelength: 5.14 μm) pointing toward the outer wall of a graphite tube inside the cavity through a CaF₂ window and by a Pt-Rh thermocouple in contact with the graphite cavity wall. At the exit of the 4 tubes, the exhaust gas-solid flows were collected and mixed together. The resulting gas temperature was about 373K, then the products were further cooled down and flowed through a filter bag to separate carbon particles. The pressure was monitored by pressure sensors placed at each tube entrance and was regulated with the use of a vacuum pump. Pressure monitoring allowed the detection of tube blocking mainly due to thermophoretic deposit at the tube outlet. The filtered gas was then analyzed to determine the gas composition. A continuous analyzer permitted to monitor the concentrations of H₂ and CH₄. The methods used for H₂ and CH₄ analysis were thermal conductivity and non-dispersive infrared detection, respectively. A gas chromatograph also measured online the outlet concentration of CH₄, C₂H₆, C₂H₄, C₂H₂, and H₂. The chromatograph (Varian CP 4900) was equipped with 2 columns: MolSieve 5A PLOT for H₂ and CH₄, and PoraPLOT U for light hydrocarbons (C₂H_y). The chromatography analysis was based on thermal conductivity detection and the carrier gas was argon, also used as buffer gas during methane cracking experiments.

2.2. Experimental results

For each experimental condition, the following parameters were calculated:

- The space time (Nauman, 2008) of the gas species is calculated by dividing the volume V_r of the isothermal part of the tubes (part inserted in the graphite cavity) by the volumetric inlet flow-rate of argon and methane at the actual tube temperature and pressure (Q_0). It gives a characteristic reaction time even if chemical expansion is not included.

$$\tau = \frac{V_r}{Q_0} \quad (2)$$

- The CH_4 conversion gives the proportion of methane that has been transformed and it is defined as:

$$X_{\text{CH}_4} = \frac{F_{0,\text{CH}_4} - F \cdot y_{\text{CH}_4}}{F_{0,\text{CH}_4}} \quad (3)$$

- The H_2 yield is the proportion of methane that has been converted into hydrogen and it is calculated from:

$$Y_{\text{H}_2} = \frac{F \cdot y_{\text{H}_2}}{2 \cdot F_{0,\text{CH}_4}} \quad (4)$$

- The C yield is the proportion of methane that has been converted into solid carbon and it is expressed as:

$$Y_{\text{C}} = \frac{F_{0,\text{CH}_4} - (F \cdot y_{\text{CH}_4} + 2 \cdot F \cdot y_{\text{C}_2\text{H}_2} + 2 \cdot F \cdot y_{\text{C}_2\text{H}_4} + 2 \cdot F \cdot y_{\text{C}_2\text{H}_6})}{F_{0,\text{CH}_4}} \quad (5)$$

where F is the total molar outlet flow-rate (including argon as buffer gas) obtained from:

$$F = F_{\text{Ar}} + F \cdot y_{\text{CH}_4} + F \cdot y_{\text{H}_2} + F \cdot y_{\text{C}_2\text{H}_2} + F \cdot y_{\text{C}_2\text{H}_4} + F \cdot y_{\text{C}_2\text{H}_6} \quad (6)$$

Eq. (6) assumes that other species different from Ar, CH_4 , H_2 , C_2H_2 , C_2H_4 , C_2H_6 were not present in the off-gas. This assumption was confirmed by gas chromatography analysis. The total molar flow-rate was also determined with a mass-balance on H, resulting in values about 5% higher than the ones obtained from Eq. (6). Resulting errors on methane conversion and on H_2 and C yields were thus estimated based on a differential calculus.

This set of indicators was the foundation of the discussion below.

2.3. Influence of the temperature

A maximum operation temperature of 2073K has been achieved. In Fig. 4, CH_4 conversion and C_2H_2 mole fraction are plotted versus space time for different temperatures (1740K, 1823K, 1973K, and 2073K). The methane mole fraction in the inlet gas is kept constant at 20% (the rest being Ar). The total gas flow-rate is changed, which thereby determines the space time of the gas. The influence of temperature is noteworthy: the higher the temperature, the higher the conversion for a given space time. For a 11 ms space time, CH_4 conversion is 62%, 79%, 93%, and 100% at 1740K, 1823K, 1973K, and 2073K, respectively. The CH_4 conversion is complete for temperatures higher than 1823K and space times higher than 25 ms. Concerning C_2H_2 mole fraction in the off-gas, it seems to be more affected by space time than by temperature. The lowest C_2H_2 concentrations are reached for the highest space times.

2.4. Influence of the space time

The influence of space time was studied at a given temperature (1823K) for a constant CH_4 mole fraction in the feed gas mixture (10%). Space times between 15 and 70 ms were considered (Fig. 5). In order to change the space time, flow-rates were modified. The first conclusion is that the CH_4 conversion and the H_2 yield are improved when increasing the space time. A more detailed analysis of the results also gives a scheme of the methane decomposition sequence. For space times between 15 and 18 ms, the H_2 yield increases due to a better CH_4 decomposition rate (the off-gas mole fraction of CH_4 decreases), while the off-gas mole fraction of C_2H_2 slightly increases. It seems that methane is converted into acetylene, thus releasing 1.5 mole of H_2 per mole of CH_4 converted. For higher space times, the H_2 yield is enhanced due to acetylene decomposition. Acetylene constitutes a reaction intermediate as discussed previously. Similar trends are observed in Fig. 4. For the lowest temperatures (1740K and 1823K), C_2H_2 off-gas concentrations present a maximum whereas C_2H_4 decreases quite monotonously for higher temperatures most probably because the maximum is reached for shorter space times. This suggests that C_2H_2 formation (CH_4 decomposition) is faster at high temperatures. Carbon yield is

also reported in Fig. 5 and it can be observed that the decrease in the C₂H₂ off-gas mole fraction corresponds closely to an increase in carbon yield. C₂H₂ is thus converted into carbon black and H₂. Hydrogen and carbon yields are two interesting parameters that permit to follow and quantify the achievement of the methane dissociation process: namely the co-production of hydrogen and carbon black.

Error bars on Y_C resulting from the uncertainty on F (Eq. (6)) are reported in Fig. 5 and they obviously increase when the inlet methane flow-rate increases (i.e. the space time decreases). For clarity reasons, error bars for the other parameters are not plotted. Anyway, the highest relative uncertainties were observed for Y_C.

A typical carbon mass balance showed that about half of the initial carbon content in the feed was found in the form of C₂H₂ at the reactor exit, 2% was found as particles in the filter, 34% in the tubes (mainly thermophoretic carbon deposit), 3% in the non-converted CH₄, the rest being attributed to other hydrocarbons and un-removed deposit. The CB showed primary particle sizes between 10 and 100 nm, which is comparable to commercial conductive carbon blacks (TIMCAL E250G, 20-40 nm). Up to 10% of thermal efficiency was reached at laboratory scale (Rodat et al., 2009c). These promising results led us to think about a potential industrial application. Consequently, a preliminary process study was performed.

3. Process analysis at 55 MW scale

3.1. Power transfer from the sun to the reactants by the solar concentrating system

A process analysis was performed at 55 MW_{solar} scale (similar to the industrial solar tower power plant in Seville, PS10). This study is based on the work of Charvin et al. (2008) for the scaling up of water-splitting thermochemical cycles. Such cycles (e.g. ZnO/Zn cycle) show similar working temperatures to the solar thermal cracking process. The solar concentrating system is a central tower configuration, as the most suitable solution for large scale production. The receiver is located at the top of the tower where the solar beam, reflected by the heliostat field, is concentrated. It is supposed that a solar concentration ratio C of 3000 is reached at the reactor entrance (for a Direct Normal Irradiation (DNI) of 1 kW/m²). This high concentration ratio may require a secondary concentrator. The fraction of the incoming solar radiation reaching the receiver is supposed to be 80% (η_{Heliostat field}=0.8), due to atmospheric absorption, shadowing and cosine effects, and guidance errors. Then, the fraction of solar power that enters the reactor amounts to 85.5% of the power reaching the receiver (η_{Receiver}=0.855) due to losses at the reactor aperture caused by concentration defects (10% of losses) and back reflection at the window (5% of losses). A sensitivity study is proposed in the following to quantify the importance of these assumptions. The reactor efficiency is determined from:

$$\eta_{\text{Reactor}} = \frac{Q_{\text{Reactor}} - (Q_{\text{Radiation}} + Q_{\text{Conduction}})}{Q_{\text{Reactor}}}$$

with Q_{reactor}, the power entering the reactor, Q_{radiation} the power lost by IR-radiation through the window, and Q_{conduction} the conduction losses through the reactor walls. The absorption efficiency of a perfectly insulated black-body cavity can be written as (Steinfeld and Palumbo, 2001):

$$\eta_{\text{Absorption}} = 1 - \frac{Q_{\text{Radiation}}}{Q_{\text{Reactor}}} = 1 - \frac{\sigma(T_{\text{Reactor}}^4 - T_0^4)}{DNI \cdot C}$$

with σ, the Stephan Boltzmann constant (5.67.10⁻⁸ W.m⁻².K⁻⁴), T_{reactor}, the reactor temperature and T₀=298.15K. Assuming 20% of conduction losses, the reactor efficiency can finally be written as:

$$\eta_{\text{reactor}} = \eta_{\text{absorption}} - 0.2 = 0.57 \text{ for a reactor temperature of } 1873\text{K.}$$

and the energy efficiency of the whole installation is:

η_{Total}=η_{Heliostat field}.η_{Receiver}.η_{Reactor}=0.39, that is to say, 39% of the incident solar radiation captured by the heliostat field is transferred to the reactants (for their heating and for the reaction). Fig. 6 illustrates these data for each components of the solar chemical plant including the heliostat field, the tower receiver and the solar reactor.

3.2. Hydrogen and carbon black production: process design

In the previous part, the power available for carrying out the reaction was estimated. Consequently, it is now possible to determine the production capacity of a first process design (Fig. 7). A 3 modules reactor at the top of a tower is envisaged with three different apertures and dedicated heliostats fields (North, East, and West fields). Secondary concentrators must be used. Each tower is expected to operate at about 11 MW_{solar} (divided in the three modules). A tubular reactor is being designed to work with turbulent flows (instead of laminar, as it was done experimentally). This will improve both heat transfer and CB transportation. In addition, the objective is to maintain a sufficiently high residence time (about 100 ms) to reach a satisfactory chemical conversion (see Fig. 5).

The feed is introduced in the reactor at 298K. It is a mixture of 50% methane (fresh and recycled) and 50% hydrogen (from PSA) pre-heated up to 1173K by the hot products. The CH₄ conversion in the reactor at 1873K is assumed to be 90% and it is supposed that only hydrogen is produced ($Y_{H_2}/X_{CH_4}=1$). Then in order to reach complete CH₄ conversion the unconverted hydrocarbons must be recycled at the reactor exit, which requires a gas separation unit (after the gas-particle separation). Pressure swing adsorption (PSA) is preferred for separating hydrogen from the other gaseous species. The solar power available in the reactor ($P_{Available\ in\ the\ reactor}=21.5\ MW$) permits to heat the reactant from 1173K to the reaction temperature and to provide the power needed for the endothermic cracking reaction. This determines the possible methane flow-rate in the feed (F_{0,CH_4}) by solving the following equation:

$$P_{Available\ in\ the\ reactor} = \int_{1173K}^{1873K} F_{0,H_2} \cdot C_{pH_2}(T) \cdot dT + \int_{1173K}^{1873K} F_{0,CH_4} \cdot C_{pCH_4}(T) \cdot dT + F_{0,CH_4} \cdot X_{CH_4} \cdot \Delta H(1873K) \quad (7)$$

with $F_{0,i}$ the inlet molar flow-rate of species i (mol/s), $C_p(T)$ the heat capacity of species i (function of T, J/mol.K) and $\Delta H(1873K)$ the reaction enthalpy (Eq. 1) at 1873K (J/mol).

At the exit of the reactor, the products are cooled down by the reactants and further to enter the filtering device at 473K. The carbon black is separated and the gaseous products are compressed and cooled down before entering the PSA system. This system is supposed to produce pure hydrogen with 80% recovery (20% of the initial hydrogen content is released with the off-gases, that is to say, it is not separated). The PSA off-gases are recycled for reaching complete methane conversion, which permits to overcome kinetic limitations responsible for unconverted gaseous species. A production of 5 t/h of carbon black and 1.7 t/h of hydrogen is obtained (for 6.7 t/h of fed methane). An average operation time of 2000 h per year at nominal power is chosen. It was evaluated that the possible exergy recovery (from products cooling) can largely compensate the compression work (that represents the main exergy requirements). Consequently, the plant is supposed autonomous and thus, neither electricity purchases nor electricity sales are considered. An economic analysis was conducted from a spreadsheet edited by DOE (2004). The same assumptions as the ones used by Charvin et al. (2008) are made regarding the size and cost of the solar concentrating system. The total investment cost is supposed to be the same (16 M\$). Fig. 8 provides the hydrogen production costs versus the carbon selling price (natural gas price of 0.24\$/Nm³ (6\$/GJ (HHV)) for reference year 2005). The cost of hydrogen produced by SMR (Steam Methane Reforming) is also reported (1 \$/kg (Muradov and Veziroglu, 2008)). The reference case is plotted for a 15% IRR (Internal Rate of Return) and 16 M\$ of investment. It shows lower H₂ production costs than the ones reported by Dahl et al. (2004a) for a solar installation about half the size of the present case. Thus, a second case is plotted with a 15% IRR and a doubled investment (32 M\$). As a result, the H₂ production costs are similar to the ones of Dahl et al. A sensitivity study was also achieved to highlight the influence of the heliostat field efficiency. If it decreases from 0.8 to 0.65, the hydrogen production drops to 1.4 t/h and the hydrogen production price rises from 0.84 to 1.22 \$/kg for a carbon black selling price of 0.7 \$/kg. The optimization of the concentrating system is thus a very strong improvement factor. For the reference case, solar hydrogen production becomes competitive with SMR at a carbon black selling price of 0.7 \$/kg, which was a typical price of standard carbon black in 2007 (Adams, 2007). Accordingly, the investment for such a solar plant should not exceed 16 M\$ for being competitive with current non-renewable process.

4. Conclusion

Thermal methane dissociation was carried out successfully in a prototype-scale solar reactor operating in the temperature range 1740K – 2070K. The influence of two main parameters, temperature and space time, on the reactor performances was stressed. Increasing the temperature permits to enhance methane conversion. Nevertheless, it is important to favour long residence times to lower the C₂H₂ off-gas content and to increase the carbon yield. In addition, a process analysis for a 55 MW solar tower plant was outlined and the production was estimated to be 1.7 t/h of hydrogen and 5 t/h of carbon black. An economic evaluation showed that the hydrogen production cost can be competitive to the conventional steam methane reforming if the CB is sold at the current market price for a 16 M\$ investment. A 50 kW solar reactor is now developed to provide further information on the process at a larger scale, especially concerning the carbon black properties with respect to the commercial standards.

Acknowledgments

This study was funded by the European Project “Solhycarb” (FP6, Contract SES-CT2006-19770). The authors wish to thank J.L. Sans, M. Garrabos, and O. Prévost for their contribution to experimental campaigns.

Nomenclature

C	Solar concentration ratio
$C_{p,i}(T)$	Heat capacity of species i (function of T, J/mol.K)
DNI	Direct Normal Irradiation (W/m ²)
F	Total molar flow-rate (mol/s)
F _i	Molar flow-rate of species i (mol/s)
F _{0,i}	Inlet molar flow-rate of species i (mol/s)
ΔH°	Standard reaction enthalpy (J/mol)
Q ₀	Inlet gas flow rate (m ³ /s)
T	Absolute temperature (K)
V _r	Reactor volume (m ³)
X _{CH₄}	Methane conversion
Y _C	Carbon yield
Y _{H₂}	Hydrogen yield
y _i	Mole fraction of species i at the exit
Greek letters:	
σ	Stephan Boltzmann constant (5.67.10 ⁻⁸ W.m ⁻² .K ⁻⁴)
τ	Mean residence time (s)

References

- Abanades, S., Flamant, G., 2008. Hydrogen production from solar thermal dissociation of methane in a high-temperature fluid-wall chemical reactor. *Chem. Eng. Process.: Process Intensif.* 47, 490–498.
- Adams, R., 2007. Booming world carbon black demand but price rises fail to keep pace with rising gas & feedstock costs. *Focus on Pigments* 3, 1-2.
- Back, M.H., Back, R.A., 1983. Thermal decomposition and reactions of methane. *Pyrolysis. Theory and industrial practice*, Academic Press, New York, 1-24.
- Billaud, F., Guéret, G., Weill J., 1992. Thermal decomposition of pure methane at 1263 K. Experiments and mechanistic modelling. *Thermochim. Acta* 211, 303–322.
- Charvin, P., Abanades, S., Lemort, F., Flamant, G., 2008. Analysis of solar chemical processes for hydrogen production from water splitting thermochemical cycles. *Energy conversion & management* 49, 1547-1556.
- Dahl, J.K., Buechler, K.J., Finley, R., Stanislaus, T., Weimer, A.W., Lewandowski, A., Bingham, C., Smeets, A., Schneider, A., 2004a. Rapid solar-thermal dissociation of natural gas in an aerosol flow reactor. *Energy* 29, 715–725.
- Dahl, J.K., Buechler, K.J., Weimer, A.W., Lewandowski, A., Bingham, C., 2004b. Solar-thermal dissociation of methane in a fluid-wall aerosol flow reactor. *Int. J. Hydrogen Energy* 29, 725–736.
- DOE (Department of Energy), 1999. A multi-year plan for the hydrogen R& D program. Rationale, structure and technology roadmaps. Office of Power Delivery and Office of Power Technologies, US Department of Energy.
- DOE, 2004. DOE Spreadsheet download at http://www.hydrogen.energy.gov/h2a_production.html.
- Donnet, J.B., Bansal, R.C, Wang, M.J., 1993. *Carbon Black*, Second Edition, New York: Marcel Dekker.
- Hirsch, D., Epstein, M., Steinfeld, A., 2001. The solar thermal decarbonization of natural gas. *Int. J. Hydrogen Energy* 26, 1023-1033.
- Hirsch, D., Steinfeld, A., 2004. Solar hydrogen production by thermal decomposition of natural gas using a vortex-flow reactor. *Int. J. Hydrogen Energy* 29, 47–55.
- Kogan, M., Kogan, A., 2003. Production of hydrogen and carbon by solar thermal methane splitting. I. The unseeded reactor. *Int. J. Hydrogen Energy* 28, 1187–1198.
- Kogan, A., Kogan, M., Barak, S., 2004. Production of hydrogen and carbon by solar thermal methane splitting. II. Room temperature simulation tests of seeded solar reactor. *Int. J. Hydrogen Energy* 29, 1227–1236.
- Muradov, N., Veziroglu, T.N., 2008. “Green” path from fossil-based to hydrogen economy: An overview of carbon-neutral technologies. *Int. J. of Hydrogen Energy* 33, 6804-6839.
- Nauman, E.B., 2008. Residence time theory. *Ind. Eng. Chem. Res.* 47, 3752-3766.
- Olsvik, O., Rokstad, O.A., Holmen, A., 1995. Pyrolysis of methane in the presence of hydrogen. *Chem. Eng. Technol.* 18, 349-358.
- Rodat, S., Abanades, S., Coulié, J., Flamant, G., 2009a. Kinetic modelling of methane decomposition in a tubular solar reactor. *Chemical Engineering Journal* 146, 120-127.
- Rodat, S., Abanades, S., Sans, J.L., Flamant, G., 2009b. Hydrogen production from solar thermal dissociation of natural gas: development of a 10 kW solar chemical reactor prototype. *Solar Energy* 83, 1599-1610.
- Rodat, S., Abanades, S., Flamant, G., 2009c. High-Temperature Solar Methane Dissociation in a Multitubular Cavity-Type Reactor in the Temperature Range 1823-2073 K. *Energy & Fuels* 23, 2666-2674.
- Steinfeld, A., Palumbo, R., 2001. *Encyclopedia of physical science & technologie*, R.A. Meyers Ed., Academic Press. 15, 237-256.
- Trommer, D., Hirsch, D., Steinfeld, A., 2004. Kinetic investigation of the thermal decomposition of CH₄ by direct irradiation of a vortex-flow laden with carbon particles. *Int. J. Hydrogen Energy* 29, 627–633.

Wyss, J., Martinek, J., Kerins, M., Dahl, J.K., Weimer, A., Lewandowski, A., Bingham C., 2007. Rapid Solar-thermal Decarbonization of Methane in a Fluid-wall Aerosol Flow Reactor – Fundamentals and Application. *International Journal of Chemical Reactor Engineering* 5, A69.

Figure captions

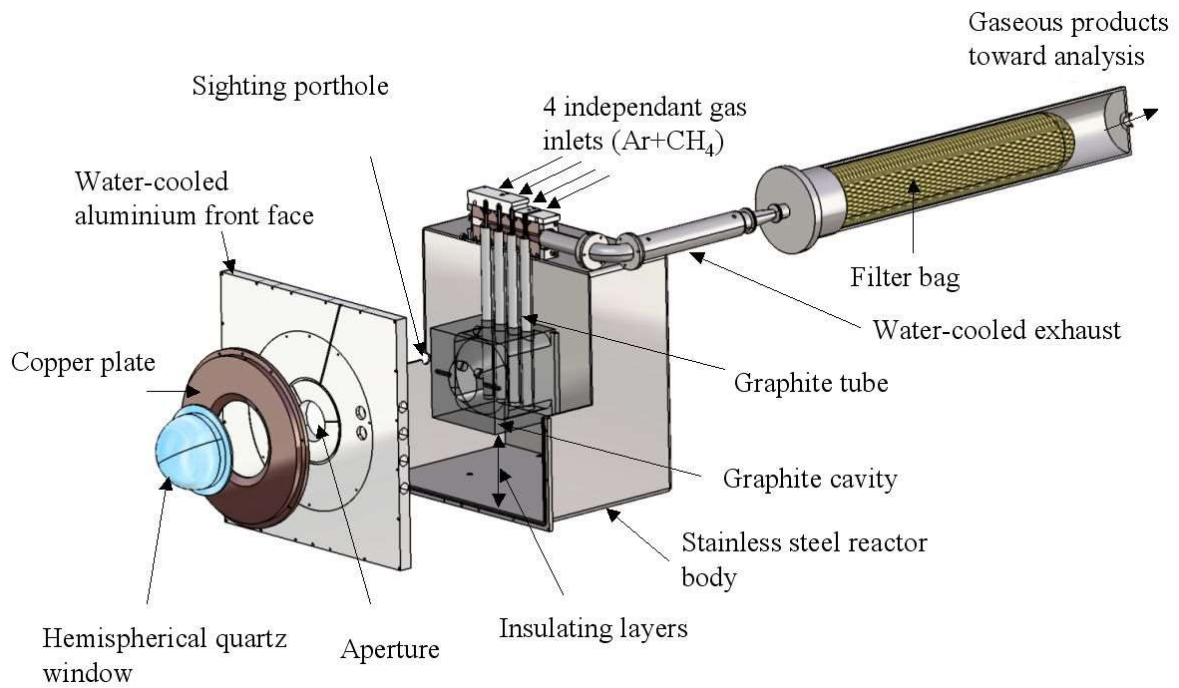


Fig. 1: Scheme of the 10 kW solar reactor and filter

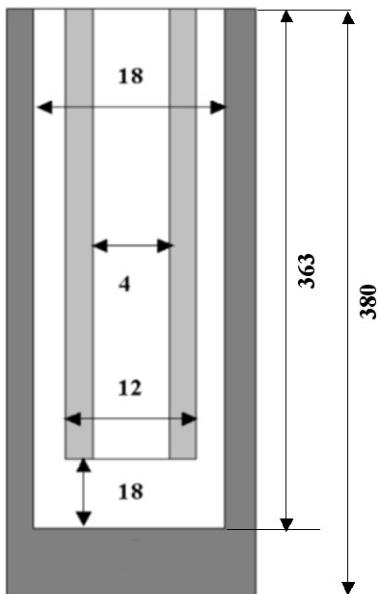
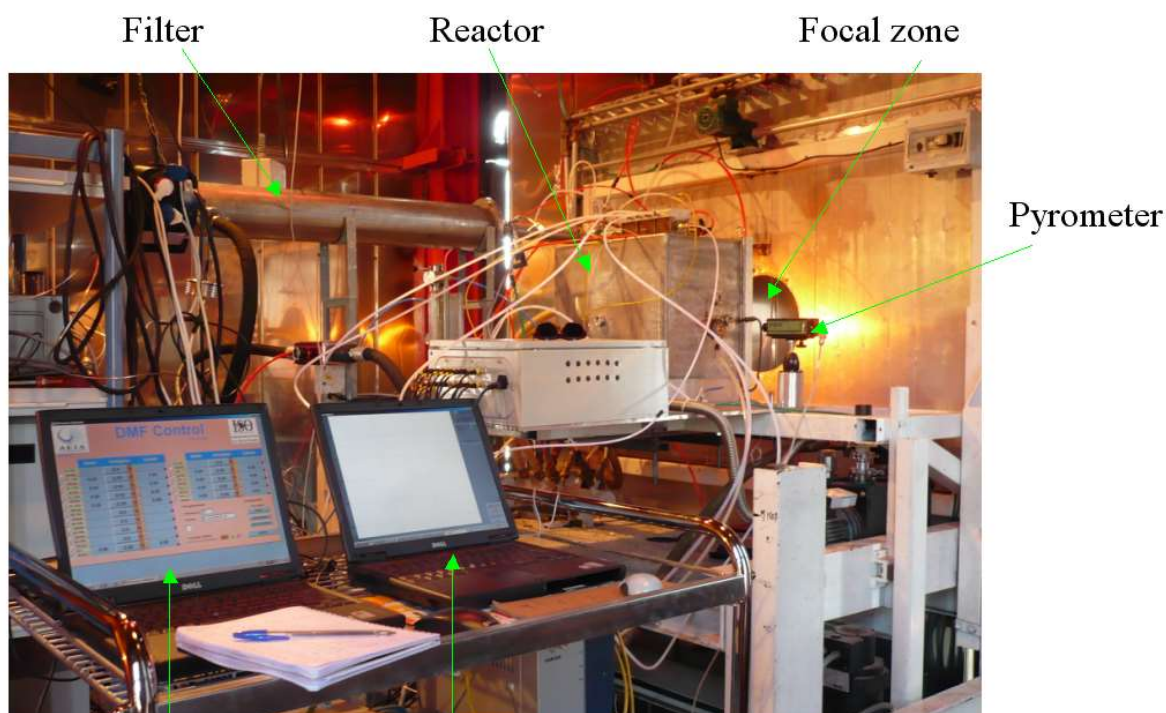


Fig. 2: Scheme of the tubular design (dimensions in mm, not scaled)



Mass-flow
controllers
monitoring

Acquisition system for
the pyrometer and the
gas chromatography

Fig 3: Photograph of the experimental set-up including the solar reactor

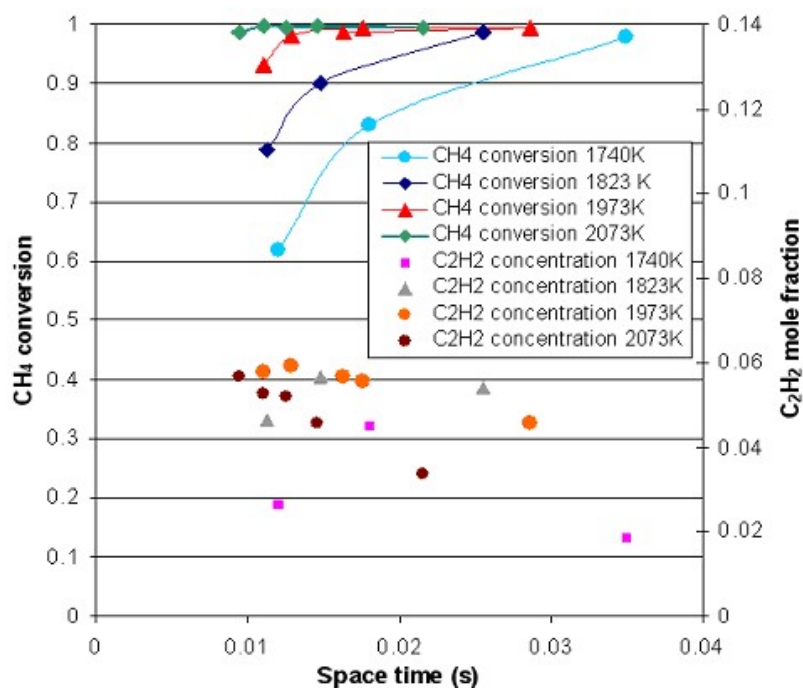


Fig. 4: CH₄ conversion and C₂H₂ off-gas mole fraction versus space time for various temperatures (20 % CH₄ in Ar)

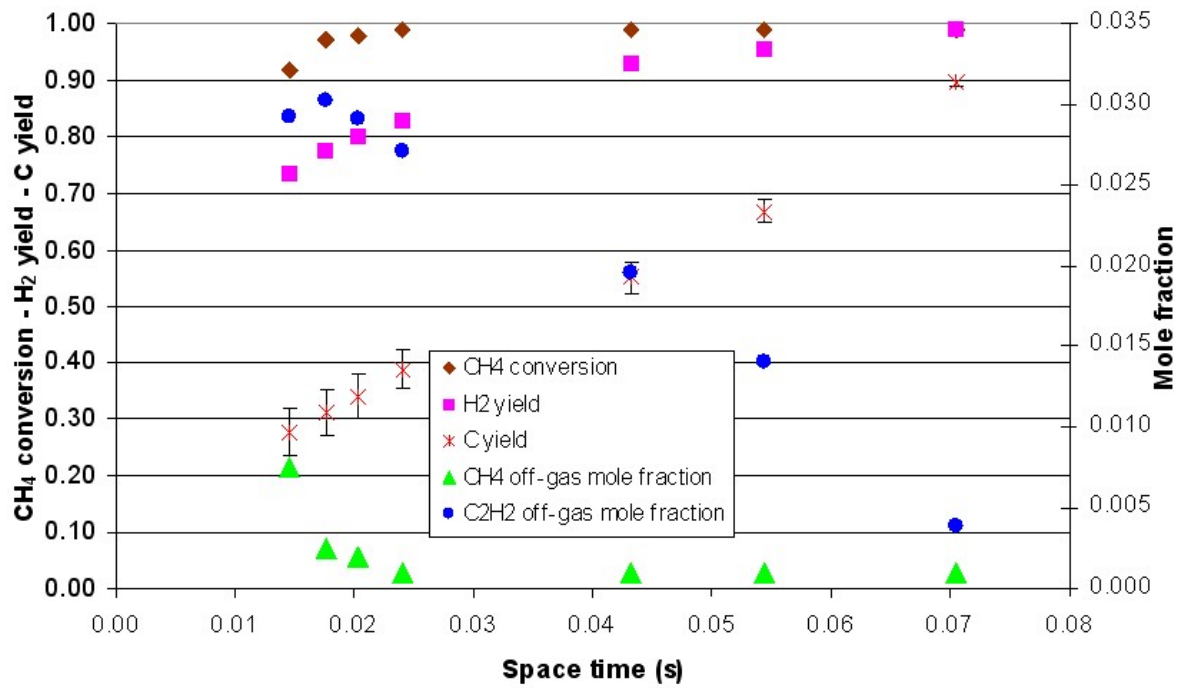


Fig. 5: CH₄ conversion, H₂ yield, C yield, CH₄ and C₂H₂ off-gas mole fractions versus space time (10 % CH₄ in Ar)

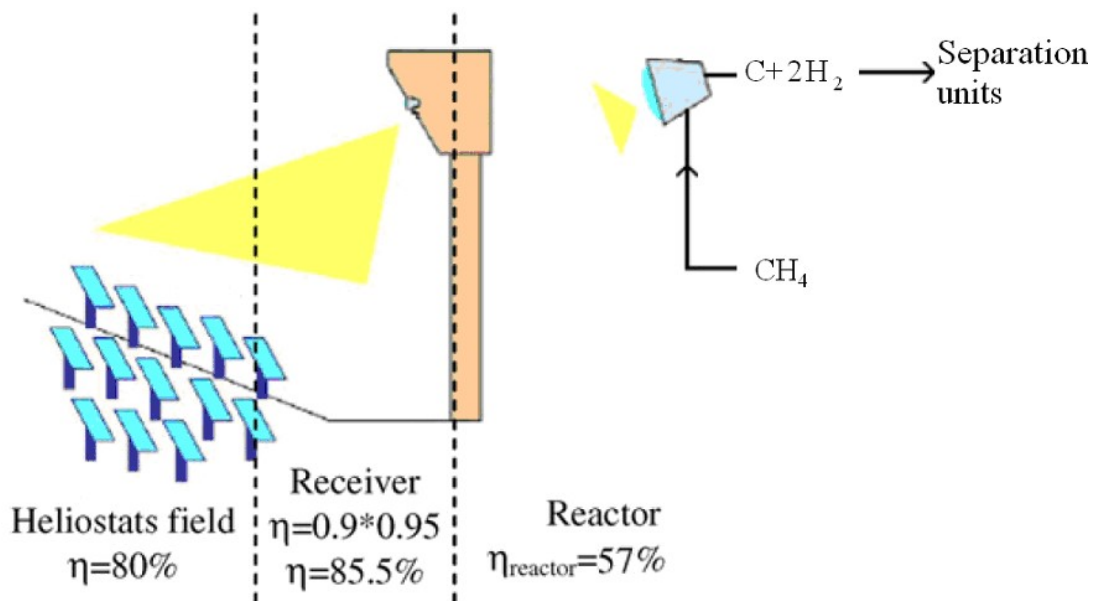


Fig. 6: Energy efficiencies related to the solar concentrating system, the receiver, and the reactor

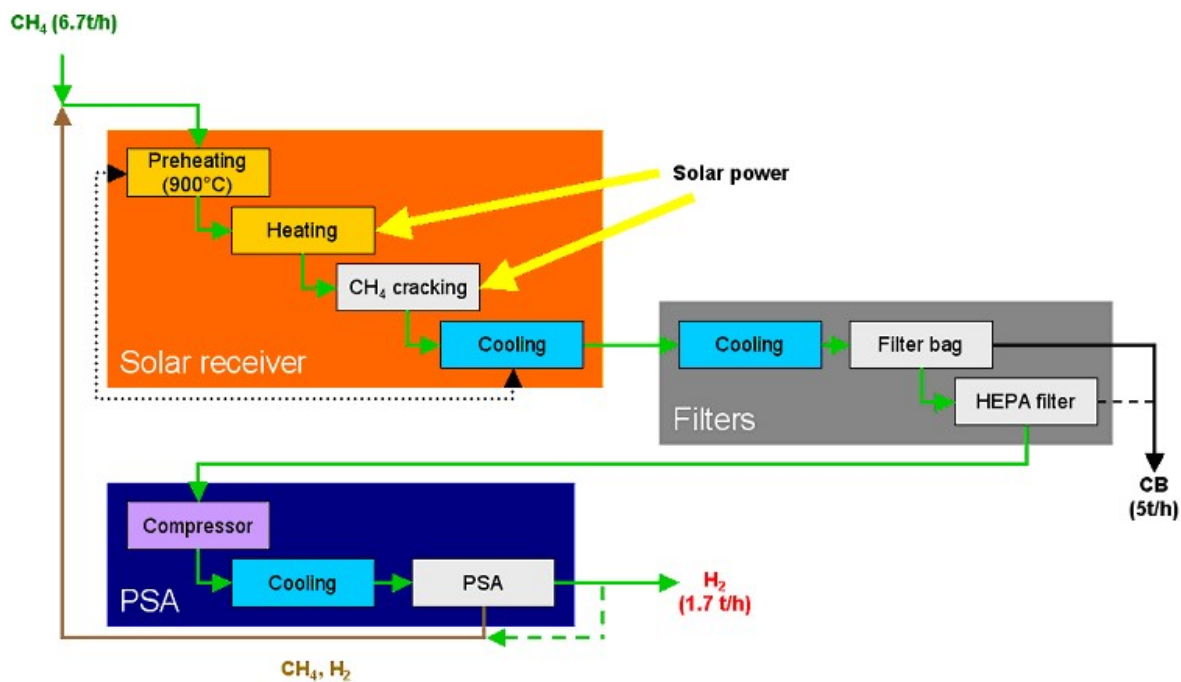


Fig. 7: Process flow diagram of the solar cracking of methane

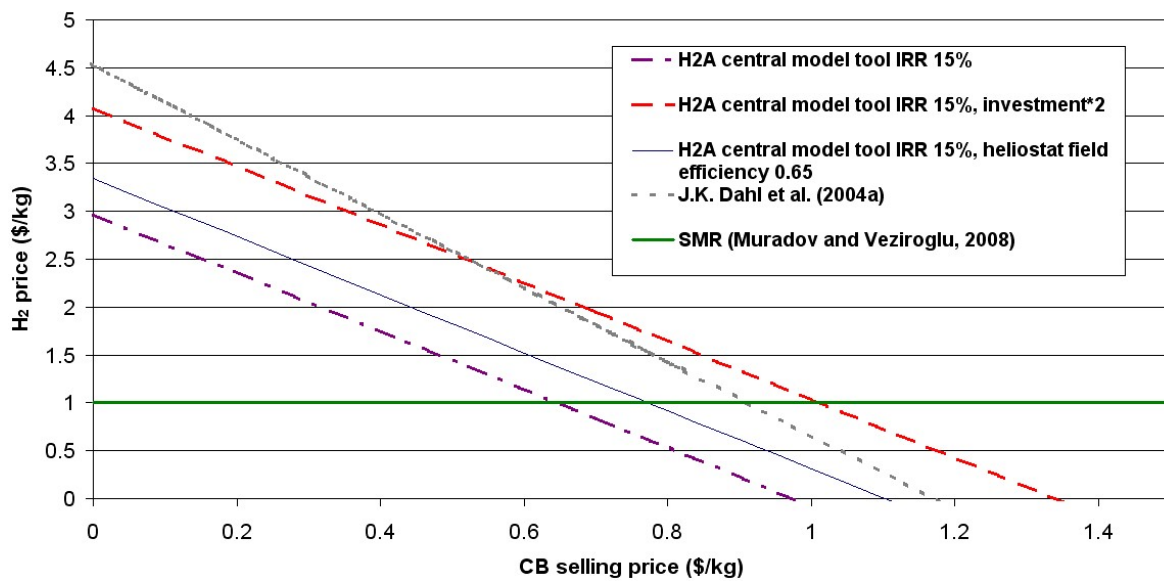


Fig. 8: Hydrogen production cost versus CB selling price